Growth and Elongation of Axons through Mechanical Tension Mediated by F luorescent-Magnetic Bifunctional Fe3O4 ·Rhodamine 6G @PDA Superparticles

Yang Wang
Jilin University First Hospital

Binxi Li
Jilin University College of Chemistry

Hao Xu
Jilin University First Hospital

Shulin Du
Jilin University College of Chemistry

Ting Liu
Jilin University First Hospital

Jingyan Ren
Jilin University First Hospital

Jiayi Zhang
Jilin University First Hospital

Hao Zhang
Jilin University College of Chemistry

Yi Liu
Jilin University College of Chemistry

Laijin Lu (✉ lulaijin@hotmail.com)
Jilin University First Hospital

Research

Abstract

Background: The primary strategy to repair the peripheral nerve injuries is to bridge the lesions by promoting axon regeneration. Thus, the ability to direct and manipulate neuronal cells axon regeneration has been one of the top priorities in the field of neuroscience. A recent innovative approach for remotely guiding neuronal regeneration is to incorporate magnetic nanoparticles (MNPs) into cells and transfer the MNPs-loaded cells into magnetic sensitive environment to response to external magnetic field. In order to realize this intention, synthesis and preparation of an ideal MNPs appears to be a challenge to overcome.

Results: In this study we design and prepare a type of novel Fluorescent-Magnetic bifunctional Fe3O4·Rhodamine 6G@polydopamine Superparticles (FMSPs) for neural regeneration therapeutics. With the help of their excellent biocompatibility and ability to interact with neural cells, our homemade FMSPs can be endocytosed into cells, transported along the axons, and then aggregated in the growth cones. As a result, the mechanical forces generated by FMSPs are capable to promote the growth and elongation of axons and stimulate gene expression associated with neuron growth under the external magnetic fields.

Conclusions: Our work demonstrates that FMSPs can be used as a novel stimulator to promote the non-invasive neural regeneration through cell magnetic actuation.

Background

Nerve regeneration and neurological functional recovery are major issues in neuroscience regarding to the treatment of peripheral nerve injuries [1]. Generally, the neuron undergoes a number of degenerative processes (Wallerian degeneration) after a peripheral nerve lesion. Benefiting from the intrinsic plasticity of the nervous system, functional reinnervation can be realize based on axonal sprout penetrating and crossing the injured site from the proximal end to their distal target. Unfortunately, unsuccessful nerve regeneration often occurs practically because the peripheral nerve lesion may cause the degeneration of distal axons and the scar infiltration at the site of the lesion, which not only pose a mechanical barrier for regenerating axons, but also act as a source of axon repellents [2]. As a result, detrimental changes, such as disorganized axonal sprouts, excess Schwann cells proliferation, and even painful neuromas, are formed. Until now, the primary strategy to repair the peripheral nerve injuries is to bridge the lesions by promoting axon regeneration. Thus, the ability to direct and manipulate neuronal cells axon regeneration is one of the top priorities in the field of neuroscience.

Recently, the mechanical characteristic of nervous system has received lots of attentions since it can be used to direct the elongation and outgrowth of axon under external mechanical tension [3–5]. In order to accurately and noninvasively deliver the external mechanical tension to axonal growth cones in vivo with controllable magnitude and duration, the application of magnetic nanoparticles (MNPs) such as Fe_3O_4 may be a promising option. Because of their magnetic properties, MNPs can be manipulated under inhomogeneous magnetic fields. For example, by incorporating MNPs into cells and placing MNPs-loaded cells under magnetic sensitive environment to response to external magnetic field gradients, the

remote guidance of neuronal regeneration is achieved. However, despite it has been reported that MNPs can be exploited to promote nerve regeneration and provide guidance for regenerating axons [6–11]. The biological behavior of MNPs being ingested by neural cells, which is the foundation of these biomedical applications, is still needs to be studied more systematically. More importantly, the genetic and molecular mechanisms which between MNPs stimulus and the biological behaviors of axon elongation are still unknown.

In this study, we demonstrate the preparation of novel Fluorescent-Magnetic bifunctional Fe_3O_4·Rhodamine 6G@polydopamine Superparticles (FMSPs) for neural regeneration therapeutics. The biocompatibility, cellular uptake mechanism, intracellular distribution and exocytosis of FMSPs are firstly characterized. Then, the influence of mechanical tension, which is created by FMSPs under external magnetic field, on the growth and elongation of axons are studied. Thirdly, gene expression profile of neural cells under mechanical tension mediated by FMSPs is investigated based on mRNA transcriptome sequencing and bioinformatics analysis. The results indicate that our homemade FMSPs can be endocytosed into neural cells via caveolae-mediated endocytosis and micropinocytosis by virtue of their excellent biocompatibility. By taking advantage of their high saturation magnetization, the mechanical tension generated by FMSPs can promote the growth and elongation of axons and stimulate gene expression associated with neuron growth under external magnetic fields.

Methods

Materials and animal care

Bovine serum albumin (BSA), fetal bovine serum (FBS), Dulbecco's Modified Eagle Medium (DMEM), neurobasal medium, NGF, penicillin/streptomycin, trypsin–EDTA, CellLight Golgi-RFP, Mito Tracker Red, ER-Tracker Red, Lyso Tracker Red, Cytochalasin D (Cyto D), tubulin beta rabbit polyclonal antibody, goat anti-rabbit IgG secondary antibody, antifade mountant with DAPI and Hoechst nucleic acid stains were obtained from Life Technologies corporation (29851 Willow Creek Road, Eugene OR 97402, USA). Methyl-β-cyclodextran (MβCD), genistein, chlorpromazine, amiloride, 2-deoxy-d-glucose (2-DG), Cell Counting Kit-8 (CCK8) were purchased from Sigma-Aldrich (3050 Spruce Street, Saint Louis, MO 63103 USA). The rabbit anti-Cdh11, rabbit anti-Csf1r, mouse monoclonal anti- β-actin and anti-mouse antibody were obtained from Santa Cruz Biotechnology (Santa Cruz, USA). The rabbit anti-Ppp1r1c antibody was obtained from Affinity (USA). The 35 mm imaging ibidi petri dishes (Ibidi, 80156) were obtained from ibidi GmbH (Am Klopferspitz 19, 82152 Martinsried, Germany) and the two-compartment microfluidic chambers were purchased from Xona microfluidics (Temecula, CA 92590, USA).

All animal procedures were performed in accordance with the Guidelines for Care and Use of Laboratory Animals of Jilin University and approved by the Animal Ethics Committee of Jilin University. All efforts were made to minimize the number of animals used and their suffering.

Synthesis and characterization of FMSPs

FMSPs were prepared according to our previous work [12]. Briefly, oleic acid (OA)-capped Fe_3O_4 nanoparticles (NPs) were synthesized following the thermal decomposition method [13]. The average diameter of the as-prepared Fe_3O_4 NPs is 5.8 nm. Subsequently, OA-capped Fe_3O_4 NPs dispersed in toluene and water containing sodium dodecyl sulfate (SDS) and Rhodamine 6G were mixed to form the oil-in-water (O/W) microemulsion. Fe_3O_4 superparticles (SPs) with an average diameter of 50 nm were produced after the evaporation of toluene [14, 15]. At last, polydopamine (PDA) was coating on the surface of Fe_3O_4·Rhodamine 6G SPs via the oxidation polymerization of the dopamine (DA) monomers under the alkaline condition [16].

The average size, distribution, and morphology of FMSPs were studied by high resolution transmission electron microscopy (HRTEM) using a Hitachi H-800 electron microscope at an acceleration voltage of 200 kV with a CCD camera. The hydrodynamic size and Zeta potential of the FMSPs were measured through dynamic light scattering (DLS) by Zeta sizer Nano-ZS (Malvern Instruments). Magnetic property characterization of the samples was performed at 300 K in a Superconducting QUantum Interference Device (SQUID) magnetometer (MPMS-XL, Quantum Design, Inc., San Diego, CA). Fluorescence spectroscopy was performed with a Shimadzu RF-5301 PC spectrophotometer.

Cell and cell culture

To study the influence of magnetic manipulation on cellular behavior in neural cells, two neural cell types including rat adrenal pheochromocytoma cells (PC12, derived from a neuroendocrine tumor of the sympathetic nervous system which is often used as a neuronal cell model) and primary rat dorsal root ganglia (DRG) neurons were cultured. PC12 cells used in this work were purchased from the Cell Bank of the Chinese Academy of Sciences (Shanghai, China) and cultured in DMEM medium supplemented with 10% FBS, 1% antibiotics (100 U/mL penicillin and 100 μg/mL streptomycin) [17, 18]. Primary DRG neurons were isolated from Sprague-Dawley rats (age 1–3 day) as described previously [19, 20], and maintained in neurobasal medium supplemented with 2% B27, 2 mM L-glutamine, 0.5% antibiotics (penicillin/streptomycin) and 50 ng/ml NGF. All cultures were conducted in an incubator at 37 °C in a humidified atmosphere with 5% CO_2. Details of primary DRG neurons extraction are presented in Additional file 1: Supplementary Information.

PC12 cells were used for cellular behaviors studies of the internalization of FMSPs, morphology analysis and to examine magnetic guidance outgrowth of neurites in directional orientation. DRG neurons were used as a model for examining magnetic tension via FMSPs interactions that stimulates the growth and elongation of axons at the single cell level.

Cytotoxicity assay

The CCK8 assay was used to examine the cytotoxicity of FMSPs. PC12 cells were seeded in 96-well plates at 1×10^4 cells per well and incubated for 24 h. Different concentrations of FMSPs (0, 20, 50, 80, 100, 200 μg/ml) were added and incubated for another 24 h. Afterwards, the medium in each well was replaced with 90 μl serum free medium and 10 μl CCK8. After 4 h incubation, the absorbance of each well

was measured at 450 nm using a Synergy HT microplate reader (Bio-Tek, Winooski, VT, USA). The survival rate of cells without FMSPs in the control wells were assumed to be 100%. Cell viability was derived through an absorbance percentage relative to the control cells.

Quantification of internal FMSPs per cell

The cells were seeded in 6-well plates (5×10^5 cells per well) incubated 24 h. After that, the cells were treated with FMSPs (10 µg/ml) for 4 h, and washed twice with cold PBS containing deferoxamine in a concentration of 1 mM to exclude the iron that was non-specifically attached to the cell membranes rather than taken up into the cells. Then the cells were collected and counted. The amount of iron inside the cells in samples was measured by ICP-AES measurements with a PerkinElmer Optima 3300DV. Based on the number of cells in the samples we can calculate the mass of iron per cell on average. From the density (ρ, 5.17 g/cm^3) and volume (V, quasi-spheres with an average diameter of 50 nm) of the Fe_3O_4 SPs core of FMSPs, we can calculate the mass of each Fe_3O_4 SPs core and the mass of iron in each FMSPs. The number of FMSPs in each cell (nFMSPs cell) can be obtained by dividing the mass of iron in each cell by the mass of iron in each FMSPs.

Immunofluorescence staining

For immunocytochemistry, after 4 h FMSPs incubation, PC12 cells were washed twice with PBS to remove free-floating FMSPs and fixed for 30 min with 4% paraformaldehyde, permeabilized with 0.1% Triton X-100 for 10 min, and blocked with 2% BSA for 1 h at room temperature. The cells were labeled with tubulin beta rabbit polyclonal antibody at 2 µg/ml in 0.1% BSA and incubated for overnight at 4 °C and then labeled with goat anti-rabbit IgG secondary antibody with Alexa Fluor 594 conjugate (Ex/Em: 590/617 nm), a dilution of 1:2000 for 2 h at room temperature. Nuclei were stained with DAPI (Ex/Em: 405/430–470 nm).

Cellular uptake kinetics

To study the effect of FMSPs concentration on cellular uptake, PC12 cells were incubated with FMSPs at different concentrations, ranging from 5 to 20 µg/ml (5, 10, 15, 20 µg/ml). To study the effect of incubation time on internalization of FMSPs, PC12 cells were incubated with FMSPs for 1, 2, 3, 4, 5 and 6 h. PC12 cells were seeded and incubated in 35 mm glass-bottom dishes (5×10^5 cells per dish) for fluorescence microscopy imaging or in 6-well plates (5×10^5 cells per well) for fluorescence activated cell sorter (FACS) analysis. Fluorescence microscope (IX51, Olympus Corporation, Tokyo, Japan) were used to examine the time and concentration-dependent uptake and the intracellular fluorescent intensity of FMSPs was qualitative observed. As for the FACS analysis (FACSAria⬛, Becton, Dickinson and Company, NJ, USA), the fluorescence intensity in cells was quantitative measured with laser excitation at 561 nm and emission filtered at 582 nm, with 15 nm band width, 10 000 events were collected for each sample.

In a separate experiment, the energy-dependent uptake was performed with low temperature incubation and ATP depletion treatments. PC12 cells were precooled at 4 °C or pretreated with 2-DG (50 mM for 45 min, create an ATP-depleted environment by interfering carbohydrate metabolism) at 37 °C, then

FMSPs were added and incubated for another 4 h. Intracellular fluorescence intensity of FMSPs was detected using fluorescence microscope and FACS.

Cellular uptake pathways

The fluorescence microscopy, FACS and TEM were used to study the exact uptake mechanism of FMSPs. Different endocytosis inhibitors were used to determine which pathway was mainly involved in the uptake of FMSPs according to the description in previous publication [21]. 2 mM of MβCD (depleting cholesterol from the cell membranes) and 50 μg/ml of genistein (inhibitor of tyrosine protein kinase blocking the phosphorylation of caveolin-1) were used to inhibit caveolae-mediated endocytosis. 10 μg/ml of chlorpromazine (inhibiting clathrin-coated pit formation) was used to inhibit clathrin-mediated endocytosis. 50 μM of amiloride (interfering with membrane Na+/H + ATPase) and 5 μM of Cyto D (inhibiting F-actin polymerization) were used to suppress the micropinocytosis. PC12 cells were pretreated with inhibitors for 45 min, FMSPs (10 μg/ml) were then added and co-incubated for an additional 4 h prior to fluorescence microscopy and FACS analysis. The cells not incubated with FMSPs served as negative control group and the group which was only treated by FMSPs was used as positive control.

Finally, TEM (EP 5018/40/Tecnai Spirit Biotwin 120KV, FEI Czech Republic s.r.o, Holland) was used to study the successive stage of FMSPs internalization. PC12 cells were incubated with FMSPs (10 μg/ml) for 4 h. Subsequently, cells samples were harvested and observed using TEM operating at 120 kV. Details of the specimen preparation are presented in Additional file 1: Supplementary Information.

Intracellular trafficking and distribution

To further determine the intracellular trafficking and distribution of FMSPs, we assessed the colocalization of FMSPs with cellular organelles by using confocal laser scanning microscopy (CLSM, FV3000, Olympus Corporation, Tokyo, Japan) image. We used cellular organelles specific fluorescent probes, including Lyso Tracker Red (Ex/Em: 561/610−710 nm), Golgi-RFP (Ex/Em:561/580−680 nm), ER-Tracker Red (Ex/Em: 561/610−710 nm) and Mito Tracker Red (Ex/Em: 561/610−710 nm), to determine intracellular distribution of FMSPs (Ex/Em: 488/500−580 nm) by assessing colocalization of FMSPs with lysosomes, Golgi apparatus, endoplasmic reticulum, and mitochondria, respectively. The experimental process was performed according to the manufacturer's instructions (http://www.thermofisher.com). The images were captured at a 60 × oil immersion objective with 3.2 × zoom magnification. Twenty different visual fields of each sample were analyzed and triplicate experiments were done. The colocalization of FMSPs with cellular organelles was analyzed by image analysis software Image J (http://rsb.info.nih.gov/ij/). Subsequently, as an additional validation experiment, the TEM was used to directly observe the distribution and localization of FMSPs in the cellular ultrastructure.

Exocytosis of internalized FMSPs

The exocytosis of internalized FMSPs was studied using FACS. After 4 h pre-incubation with FMSPs, the cells were washed by PBS for three times and cultured in fresh culture media without FMSPs. After further incubation for 2, 4, 8, 12 and 24 h, the cells were collected for FACS analysis to measure the intracellular mean fluorescence intensity.

Magnetic field preparation and quantification of magnetic forces

One perpetual cuboid neodymium magnet (NdFeB N48, cuboid side 50 mm × 30mm × 10 mm) was applied to the right side of the culture dish to generate a gradient magnetic field to the cells at the center of the dish (Fig. 1a). The magnetic field was simulated by means of numerical field calculations using the software Comsol Multiphysics 4.3b (Comsol Multiphysics GmbH, Goettingen, Germany). A digital Gauss-meter (Scientific Equipment Roorkee, DGM-204) was used to measure the magnetic flux density induced by the setups of neodymium magnet.

The exact explanation of quantification of magnetic forces is as described in reference [6, 22]. A magnetic particle within a magnetic flux density gradient (∇B) experiences magnetic forces F direct towards regions with higher filed density due to its magnetic momentum (m):

$$F = (m \cdot \nabla)B \qquad \text{Eq.(1)}$$

In our experimental set-up, derivative of flux density B(T) along the magnetic field gradient inside the magnetic applicator is dB/dr (T/m). Superparamagnetic nanoparticles in gradient magnetic fields exert force is due to a combination of parameters. As we find a value of FMSPs saturation magnetization M_s, the density ρ and volume V, we can assume the net force F_{FMSP} of FMSP:

$$F_{FMSP} = m_s \frac{dB}{dr} = \rho V M_s \frac{dB}{dr} \qquad \text{Eq.(2)}$$

Mass of iron up-taken by PC12 cells was measured and the number of FMSPs per cell (nFMSPs cell) can be calculated. A single cell will be thus subject to a force F_{cell} given by the F_{FMSP} multiplied for the number of FMSPs in the cell:

$$F_{cell} = n_{cell}^{FMSPs} \cdot F_{FMSP} \qquad \text{Eq.(3)}$$

Neurite orientated growth assay

PC12 cells were used to examine magnetic guidance outgrowth of neurites in directional orientation. PC12 cells were seeded in ibidi petri dishes. After 24 h from seeding, cells were treated with 10 µg/ml of

FMSPs and incubated again for 4 h to allow the FMSPs to interact with cells. The dishes were then put inside the magnetic applicator. After 24 h, the outgrowth of neurites was induced under external magnetic force, the angle θ between the long axis of a neurite and the direction of the magnetic field (Fig. 1b) as well as the neurite length were measured. Neurite orientation was quantified as an orientation index (Oi), which was defined as Oi = cos(θ), with 0 < θ < π (when θ is 0, neurites with their long axis parallel to the magnetic field vector will have an Oi of + 1, while when θ is π, neurites opposite to the magnetic field vector will have an Oi of -1. Randomly oriented neurites will have an average Oi of 0).

Four experimental groups were tested: (1) treatment group, cells treated with both FMSPs and magnetic field ($FMSPs^+$, M^+), (2) FMSPs control group, treated with FMSPs and no magnetic field ($FMSPs^+$, M^-), (3) magnetic field control group, without FMSPs and treated by magnetic field ($FMSPs^-$, M^+) and (4) blank control group, without FMSPs and a null magnetic field ($FMSPs^-$, M^-). Experiments were performed in triplicate. For each experiment, 625 pictures were acquired under microscopic high-power fields (20 × objective with 2.5 × zoom) at the centers of the dishes. For each picture all of the neurites were measured. Analysis was performed by using Image J software.

Velocity measurement of DRG axonal elongation

To determine whether external magnetic forces stimulation affect growth cone motility and the rates of axonal elongation in neurons, we used the two-compartment microfluidic chambers for DRG neuronal culture. In the previous studies have demonstrated that microfluidic chambers composed of two compartments (cell-body and distal-axon compartments) interconnected by microchannels (the height of the microchannels is designed to be much smaller than the size of the cell body) can be used to separate axons from their cell bodies (Fig. 1c) [20, 23–26].

Neurons were initially plated in the left cell-body (CB) compartment, cells extend out long axons (~ 1 μm diameter) that are smaller than the microchannels and grow across the microchannels into the right distal-axon (DA) compartment after a few days. Monitor the growth of DRG neurons in a microfluidic chamber by time-lapsed imaging. During time-lapse recordings, cultures were recorded at 2.5 min/frame with differential interference contrast (DIC) optics (20 × objective with 2.5 × zoom). Time of the extending axons grew across 150-μm-long microchannels was recorded. Average elongation rates of axons were then constructed from each individual axon growth trajectory. Experiments were carried out in triplicate, more than 40 trajectories from single axon were collected and measured at each experiment.

mRNA transcriptome sequencing and bioinformatics analysis

To further determine the effects of mechanical signals mediated by FMSPs on gene expression profile in neural cells, we also performed mRNA transcriptome sequencing and bioinformatics analysis on cell samples from different experimental groups. Experiments were carried out in triplicate.

RNA extraction, cDNA library establishment and Illumina sequencing: the total RNA was isolated from cultured sample cells using TRIzol regents (Invitrogen, Carlsbad, CA, USA) and the purity, concentration and integrity of RNA were checked and controlled. The mRNA enrichment was collected by the combination of oligo (dT)-attached magnetic beads and the ploy A tail. The mRNA interrupted fragments were synthesized into a strand of cDNA with random hexamer primers, and then the buffer solution, dNTPs and DNA polymerase were subject to synthesis of the second-strand cDNA. The purified cDNA was terminally repaired, ligated, and PCR amplified to obtain the final cDNA library. Illumina HiSeqTM 2000 sequencing platform was used to sequence. All sequence data was submitted to NCBI database under the project accession number PRJNA597946 (https://www.ncbi.nlm.nih.gov/sra/PRJNA597946). To ensure the accuracy of subsequent bioinformatics, the original sequencing data was first filtered to obtain high-quality clean data. Then, using Hisat2 software (version 2.1.0, https://ccb.jhu.edu/software/hisat2/index.shtml) [27], sequencing reads were aligned to the rat reference genome (ftp://ftp.ccb.jhu.edu/pub/infphilo/hisat2/data/rn6.tar.gz) to obtain high-quality sequencing data. Moreover, featureCounts software [28] (version 1.6.0) was carried out to analyze the gene expression level. Details of the quality control of the RNA extraction and the processing of raw sequencing data are presented in Additional file 1: Supplementary Information.

Screening differentially expressed mRNA: the obtained raw date were standardized with DESeq2 softwares (version 1.18.1,http://www.bioconductor.org/packages/release/bioc/html/DESeq2.html) [29], followed by pairwise comparison using Wald test in DESeq2. Differentially expressed mRNA were chosen by using P. Value < 0.05 and |logFC| >1. Gene ontology (GO) analysis was utilized to analyze the putative functions for key gene using clusterProfile in R (version 3.8.1, http://bioconductor.org/packages/release/bioc/html/clusterProfiler.html)[30]. Up-regulated differentially expressed mRNA were carried out the GO biological process functional annotation [31] and enrichment analysis, respectively. And the p-value less than 0.05 was acted as cut-off for the differential gene expression of significantly enriched GO terms.

Quantitative real-time PCR

Cell samples from different groups were washed with pre-cooled PBS three times. Cell lysis was used for total RNA extraction by adding 1 ml TRIzol reagent. The obtained RNA was reversedly transcribed into the preparation of cDNA using primeScript RT Master MIX (Takara, Dalian, China), followed by PCR amplification. PCR was used to quantify differences in the mRNA expression using PowerUp SYBR™ Green Master Mix Kit (Waltham, MA, USA), GADPH was applied as an internal control. Primers used in PCR were synthesized by Invitrogen (Shanghai, China), and the sequences are listed in Table S2 of Additional file 1: Supplementary Information. PCR reaction conditions were conducted as follows: initial denaturation at 95 °C for 10 min; 95 °C for 10 s, 60 °C for 30 s, 72 °C for 1 min, and the amplification was performed for 40 cycles; extension at 72 °C for 10 min. The multiple relationships of gene expression changes in different cells were calculated by using $2^{-\Delta\Delta Ct}$ methods. Each reaction was performed with three times.

Western Blots

Cell samples from different groups were washed with PBS, and subsequently obtained in Radio-Immunoprecipitation Assay (RIPA, Beyotime, Shanghai, China) lysis buffer. In the following, cell lysates were collected by centrifugation (12,000 rpm for 15 min at 4 °C). Total proteins were quantified using the bicinchoninic acid (BCA, Thermo, Scientific, California, USA) protein assay kit. Proteins were separated by 10% sodium dodecyl sulphate-polyacrylamide gel electrophoresis (SDS-PAGE), followed by transfer of polyvinylidene difluoride (PVDF) membranes (Millipore, Bedford, MA, USA). The solution including 5% nonfat dry milk was used to block the membranes for 1 h. Subsequently, the membranes were incubated with the primary antibodies, rabbit anti-Cdh11 (1:10000), rabbit anti-Csf1r (1:10000), rabbit anti-Ppp1r1c (1:10000), mouse monoclonal anti- β-actin (1:10000) overnight at 4 °C. After three washes in PBST buffer, membranes were incubated with anti-mouse antibody (1:5000) at 37 °C for 1 h and then washed three times in PBST. The special bands were shown using a chemiluminescence (ECL) method (Millipore, Bedford, MA, USA). TanonImage software (Tanon Science & Technology, Shanghai, China) was used to conduct grayscale analysis for the protein expression. Experiments were carried out in triplicate.

Statistical analysis

Continuous variables with normal distribution, such as cell viability, fluorescence intensity of cells, and elongation rates of axons, were represented as the mean ± standard deviation (SD). The distributions of the variables of neurite orientation index (Oi) and neurite length were found to be no normal by Kolmogorov−Smirnov test, therefore, their values were represented by median and interquartile range (Q1-Q3). Statistical significance was calculated using either one-way ANOVA (no rejection of normality) or nonparametric Kruskal-Wallis ANOVA (normality rejected). All of the analyses were conducted with SPSS program (version 18.0, Chicago, IL, USA), $P < 0.05$ was considered to be statistically significant.

Results And Discussion

Synthesis and characterization of FMSPs

Herein, homemade Fe_3O_4·Rhodamine 6G@PDA SPs (FMSPs) used in this work are fabricated by coating preassembled Fe_3O_4·Rhodamine6G SPs with PDA. HRTEM images show that FMSPs possess an uniform size with the core size of 50 nm and the PDA shell of about 10 nm (Fig. 2a, b). The PDA shell can improve the biocompatibility, physiological stability, and colloidal stability of FMSPs. The hydrated diameter measured through DLS is 93.6 nm (Fig. 2c), which is larger than that measured in TEM images, but still within the optimal range for uptake by non-phagocytic cells [32−34]. The polydispersity index (PDI) measured by DLS is 0.186, implying the excellent dispersibility of our homemade FMSPs. Zeta potential measurement of FMSPs suspended in cell culture media reveals a weak negative charge of -12.7 ± 2.3 mV, which is more favorable for their interactions with negatively charged cell membrane and subsequent uptake [10]. The magnetic curves of FMSPs are characterized by SQUID, and the saturation magnetization is 62 Am^2/kg without any evident remanence or coercivity at 300 K, suggesting the superparamagnetic property of FMSPs (Fig. 2d). Figure 2e exhibits the high magnetic responsibility of FMSPs toward external magnetic field, which is the key parameter for maximizing the force transfer

efficiency from the external magnetic field to the FMSPs-loaded cells. The optical properties of FMSPs are investigated as well. As shown in Fig. 2g, FMSPs possess a green color emission at around 556 nm under 350 nm excitation. The photograph shown in Fig. 2f further indicates their bright green fluorescence excited by the hand-hold UV lamp. PC12 cells after incubation with FMSPs exhibit a strong green fluorescence, which demonstrates that the FMSPs have an ideal capacity to label mammalian neural cells (Fig. 2h).

Minimal cytotoxicity is essential for any biomedical application. The cytotoxicity of FMSPs is firstly evaluated by standard CCK8 assay. After incubation with FMSPs for 24 h, the cell viability of PC12 cells remain above 80% at concentration range from 20 to 200 μg/ml (Fig. 3a). Measurements of cell viability after 48 and 72 h in culture demonstrate the similar trend, implying that the uptake of FMSPs do not affect cell viability and replication rate. The Additional file 2: Movie S1 show that PC12 cells are able to maintain active mitotic proliferation and neurites outgrowth after endocytosis of FMSPs. The amount of FMNPs uptake by PC12 cells is calculated by ICP-AES. After incubation with FMSPs (10 μg/ml), the cells are able to incorporate quantities of Fe up to 6.90 ± 0.07 pg/cell, corresponding to $\sim 3.73 \pm 0.036 \times 10^4$ FMSPs/cell. These data demonstrate that using 10 μg/ml as the working concentration not only guarantees extremely low cytotoxicity, but also ensures that sufficient FMSPs can be taken up by cells. The low cytotoxicity of Fe_3O_4 is one of its great advantages comparing with other MNPs [8, 22, 35, 36]. Our results are consistent with these literatures and manifest that PDA coated superparamagnetic $Fe_3O_4 \cdot$Rhodamine 6G SPs are basically noncytotoxic even under the high concentration of 200 μg/ml. Additionally, effects of FMSPs treatment on the normal differentiation capacity of DRG neuronal cells are examined as well. As a result, there is not any significant change in viability and differentiation capacity of DRG neurons can be observed even after incubation with FMSPs (10 μg/ml) for up to 72 h. DRG neurons treated by FMSPs retain their differentiation property, leading to the neurite outgrowth and complex neuronal networks formation (Fig. 3b and Additional file 3: Movie S2).

The idea of using mechanical tension mediated by MNPs to stretch the growth and elongation of axons provides a new approach for repairing neurological diseases and injuries. To this end, design and preparation of ideal MNPs appears to be a challenge to overcome. Our results suggest that FMSPs are promising candidates as biocompatible magnetic agents for magnetically-driven cell actuation.

Cellular behaviors of FMSPs internalization

The uptake behavior of FMSPs by cells is further studied. CLSM images of cells at a single focal plane exhibit the high fluorescence within the cells, verifying the internalization of FMSPs into the cells (Fig. S1 in Additional file 1: Supplementary Information). For assessing the extent of FMSPs internalization, the intracellular fluorescence intensity is measured by fluorescence microscopy and flow cytometry. As shown in Fig. S2 in Additional file 1: Supplementary Information, the cellular uptake of FMSPs depends on the FMSPs concentration in the medium. With increasing the concentration of FMSPs in the culture environment, the fluorescence intensity in cells and the intracellular amount of FMSPs increase. PC12 cells have the great uptake amount and high fluorescence levels even at low concentrations of FMSPs

(10 µg/ml). Subsequently, the influence of incubation time on the uptake of FMSPs by PC12 cells is measured by fixing the FMSP concentration (10 µg/ml) but prolong the incubation duration from 1 to 6 h. As a result, the fluorescence intensity increases rapidly within 1 h and reach a plateau after 2 h incubation (Fig. S3 in Additional file 1: Supplementary Information). According to the FACS analysis in Fig. S3f and S3g, it can be seen that the uptake of FMSPs within 1 h is extremely high, followed by a significant deceleration between 1 and 2 h, then reaches saturation after 2 h.

Previous studies reported that the endocytosis process participated in NPs cellular uptake is an energy-dependent active transport [37–42]. To better evaluate the uptake kinetics, the cellular uptake of FMSPs under low temperature (4 °C) and ATP-depleted environments (in the presence of 2-DG) are analyzed. Fluorescent images indicate that the low temperature and ATP-depletion can inhibit the cellular uptake of FMSPs (Fig. S4a-d in Additional file 1: Supplementary Information). As shown in Fig. S4e and S4f, comparing with positive control group at 37 °C, FMSPs uptake by PC12 cells under low temperature or ATP-depletion environment reduced by $91.8 \pm 0.3\%$ ($P < 0.05$) and $65.6 \pm 2.8\%$ ($P < 0.05$) respectively. This result reveals the energy-dependent characteristic of FMSPs uptake.

Since the endocytosis of NPs in non-phagocytic cells generally include caveolae-mediated, clathrin-mediated, and micropinocytosis [43, 44]. To elucidate the specific endocytic mechanism of FMSPs uptake by cells exactly, different endocytosis inhibitors are employed to identify the endocytic pathways involved in the uptake of FMSPs (Fig. 4a and 4b). MβCD and genistein are firstly utilized to inhibit the caveolae-mediated endocytosis [45]. It reveals a significant decrease in FMSPs uptake with the inhibition rates of approximately $37.9 \pm 4.3\%$ ($P < 0.05$) and $46.1 \pm 3.6\%$ ($P < 0.05$) in PC12 cells. This result suggests that the caveolae-mediated endocytosis is one pathway for FMSPs uptake. Then, chlorpromazine is employed to inhibit the clathrin-mediated endocytosis [45]. As result, no obvious inhibition of FMSPs uptake is found, indicating clathrin-mediated endocytosis do not play an important role in the uptake of FMSPs (data is not shown). At last, amiloride and Cyto D are used to suppress the micropinocytosis [46], and the inhibition rates of approximately $45.5 \pm 3.6\%$ ($P < 0.05$) and $49.6 \pm 0.6\%$ ($P < 0.05$) are observed, indicating that micropinocytosis is a primary pathway for FMSPs uptake. To look in more detail, the trafficking of FMSPs into the cells is monitored by TEM analysis. Figure 4c shows the dispersed FMSPs in the cell membrane appearing to enter the cells by caveolae-mediated endocytosis. Figure 4d shows the cluster of FMSPs appearing to enter the cells by micropinocytosis. Neither FMSPs in nuclei nor damages at the cytoplasmatic organelles are found.

CLSM is further performed to identify the biodistribution of FMSPs within nerve cells. The FMSPs intracellular distribution is evaluated via co-incubation followed by co-staining with various organelle-specific fluorescent probes (LysoTracker, ER-Tracker, Golgi-RFP, and MitoTracker) (Fig. 5a-d). Figure 5a and 5d show that the internalized FMSPs are primarily distributed in Golgi apparatus and mitochondria of PC12 cells. Accordingly, the Pearson correlation coefficient (Rr) are 0.656 ± 0.067 and 0.624 ± 0.026 respectively, suggesting the good colocalization between FMSPs and these subcellular structures. Most importantly, our FMSPs can be observed not only in cytoplasm but also in the cone growth of developing neurites. With the help of CLSM, tomographic scanning and time-lapsed imaging are performed to clearly

distinguish the intracellular distribution of FMSPs. Additional file 4: Movie S3 shows that FMSPs are transported bidirectionally within neurites, which can be detected as puncta in the growth cones, neurites, and cell bodies.

To study the exocytosis of internalized FMSPs, cells are firstly pre-incubated with FMSPs for 4 h, then washed with PBS and incubated with fresh culture media for 2, 4, 8, 12 and 24 h at 37 °C. Figure S5 in Additional file 1: Supplementary Information shows the significant decrease in intracellular FMSPs fluorescence intensity with increasing incubation time. But cells still maintain a high survival rate in the whole test period. The effective exocytosis of FMSPs further demonstrates the low cytotoxicity and high biocompatibility of FMSPs.

A comprehensive study of the neural cell behaviors on FMSPs uptake is highly indispensable for assessing the biological features and subsequent biomedical applications of FMSPs. The findings derived from this study not only provide some details on neural cell behaviors for FMSPs uptake, but also set the foundation for using the mechanical force mediated by FMSPs to guide the regeneration of axons.

Magnetic mechanical forces induce axonal outgrowth

To prove the concept that FMSPs can be exploited to manipulate the growth and development of neurites/axons under external magnetic fields. Experiments are carried out inside a constant magnetic flux density gradient generated by one perpetual cuboid neodymium magnet, which provide about 6.0 T/m of magnetic field to the cells at the center of the dish along the direction of the magnetic field gradient (Fig. S6 in Additional file 1: Supplementary Information). The homemade FMSPs used in this work have an average Fe_3O_4 core diameter of 50 nm (the volume is about 6.54×10^4 nm^3) and a saturation magnetization of 62 Am^2/kg. Since the density (ρ) of Fe_3O_4 is 5.17 g/cm^3, a single FMSP subjected to a force F_{FMSP} is calculated to be ~ 1.15×10^{-4} pN (Eq. (2)). The number of FMNPs up-taken by PC12 cells is estimated to be ~ 3.73×10^4 FMSPs per cell. Thus, the average magnetic force on single cell F_{cell} is calculated to be ~ 4.29 ± 0.042 pN (Eq. (3)).

PC12 cells loaded with FMSPs are used to examine the effect of magnetic forces on the growth of neurite under the external magnetic field. The inclination angles θ between the long axis of the neurites and the line drawn parallel to the magnetic field are measured (Fig. 6a). Neurite orientation is quantified by introducing the concept of orientation index (Oi). Figure 6a and Additional file 5: Movie S4 show that the neurites of PC12 cells treated with FMSPs (FMSPs⁺, M⁺) tend to be arranged in parallel with one another and grow preferentially along the direction of the magnetic force when the magnetic field is applied. In contrast, the neurite growth directions for the control neurons appear to be random with no preferable direction in the absence of magnetic stimulation. Furthermore, experimental evidences demonstrate that neither the FMSPs nor the magnetic field alone can influence the neurite growth direction. The value of Oi in the blank control group (FMSPs⁻, M⁻) is -0.032 (-0.571~0.604), which is not statistically significant different from that obtained when the magnetic field is applied (FMSPs⁻, M⁺; Oi =-0.027, P = 0.493) or

cells are treated with FMSPs (FMSPs$^+$, M$^-$; Oi =-0.076, P = 0.580) alone (Fig. 6b). In contrast, Oi in the treatment group (FMSPs$^+$, M$^+$) is 0.726 (0.171~0.936), which is much higher than that in other groups (P < 0.05) (Fig. 6b). Concerning the length distribution of neurites along the magnetic force direction, a trend toward statistical significance (P < 0.05) with the higher value of the neurites length for cells treated with both the FMSPs and the magnetic field (43.115 μm, 26.370~65.817 μm) compared to the control group (36.110 μm in FMSPs control group, 21.885 μm in magnetic field control group and 28.289 μm in blank control group, P < 0.05) is observed (Fig. 6c).

To determine effects of nanomagnetic force stimulation on the growth cone motility and axon elongation rate, primary DRG neurons are cultured inside microfluidic chambers. In the treatment group (FMSPs$^+$, M$^+$), neurons are dissociated and incubated in medium enriched by FMSPs under an external magnetic field with a magnetic gradient. Figure 7a and Additional file 6: Movie S5 show the magnetic force acting on the FMSPs-bound axons of DRG neurons allows growth cone to grow rapidly and directionally toward the distal-axon (DA) compartment (magnetic source) within a short time by crossing the microchannels. The growth of DRG neurons in a microfluidic chamber are monitored for more than 24 h by time-lapsed imaging, and the average elongation rate of the axons are 33.4 ± 8.6 μm/h throughout the observation period. In the control groups (FMSPs$^-$, M$^-$; FMSPs $^+$, M$^-$ and FMSPs$^-$, M$^+$) without nanomagnetic force stimulation, axons emerge out of the neuron cell bodies spontaneously and develop towards all directions without any preferred orientation (Fig. 7b-d and Additional file 7−9: Movie S6-S8). At the same time, the rates of axon growth decrease significantly in these control groups (11.1 ± 3.8 μm/h in blank control group, P < 0.05; 10.9 ± 4.2 μm/h in FMSPs control group, P < 0.05 and 9.7 ± 4.2 μm/h in magnetic field control group, P < 0.05) (Fig. 7e). Thus, it is reasonable to believe that synergic combination of FMSPs and external magnetic field can improve the motility of growth cone aligning the direction of the magnetic force and accelerate the outgrowth of axons.

The axon elongation is the result of axonal framework stretches caused by the tension from growth cone under external chemical or physical stimulations [47]. More recently, mechanical forces in the range of several pN have been reported to have the ability to influence the outgrowth process with the help of a MNPs-based technique [6, 7, 10, 11, 48]. In our system, we demonstrate that internalized FMSPs in neural cells may generate a ~ 4.29 ± 0.042 pN tension force to physically direct the neurite orientated outgrowth and the axonal elongation. Based on previous works and our findings, it is believed that upon precise control the magnitude of mechanical forces mediated by FMSPs and the duration under forces, manipulating the development of axonal is possible.

Gene expression mediated by magnetic mechanical forces

To further determine the effects of mechanical signals mediated by FMSPs on gene expression profile in neural cells, mRNA transcriptome sequencing and bioinformatics analysis on cell samples from different experimental groups are performed. The mechanism of magnetic mechanical force on promoting axonal regeneration from the perspective of genetics is further expected to elucidate. Since only the cooperation of FMSPs and magnetic fields can affect the regeneration of axons, cells from the treatment group

(FMSPs⁺, M⁺) and the blank control group (FMSPs⁻, M⁻) are selected for gene sequencing. As presented in Fig. 8a, volcano plot is used to assess gene expression variation between treatment and blank control group. After the pairwise comparison, a total of 89 mRNAs display differential expression including 43 up-regulated mRNAs. The level of expression changes for differentially expressed mRNAs is exhibited in heatmap (Fig. 8b). The GO enrichment analysis is utilized to annotate genes and analyze the biological processes of genes. From Fig. 8c it can be seen that a total of 43 up-regulated mRNAs are mainly involved in regulation of chemokine secretion process (GO: 0090197, 0090196, 0090195), central nervous system neuron differentiation and axonogenesis process (GO: 0021953, 0021952, 0021955), as well as regulation of mitotic cell cycle phase transition process (GO: 1900087, 1901990, 1902808, 1901987). Meanwhile, three target genes including Csf1r, Cdh11 and Ppp1r1c are identified and screened among the biological processes highly-correlated axon growth from up-regulated GO terms. The three identified differentially expressed mRNAs are further validated with reverse transcription-quantitative real-time PCR (RT-qPCR) analysis in PC12 cells. The expression level of Cdh11, Csf1r and Ppp1r1c are significantly up-regulated in treatment group compared with the blank control group ($P < 0.01$) (Fig. 9a-c). Furthermore, the lysates from samples are conducted the western blot. As shown in Fig. 9d-f, the protein level of Cdh11, Csf1r, and Ppp1r1c are remarkably increased in treated samples compared with the blank control sample (*$P < 0.05$, **$P < 0.01$). The findings further verify the accuracy of sequencing data and in line with the bioinformatics results.

Cdh11 gene encodes a type II classical cadherin (Cadherin-11) from the cadherin superfamily, integral membrane proteins that mediate calcium-dependent cell-cell adhesion. The expression of Cdh11 is associated in growth cones movement in the period of axonal migration [49]. Cadherin-11 is an axon growth-promoting factor, involved in growing motor and sensory axons in the mouse embryo in a previous study [50, 51]. In the regulation of axon growth, Cadherin-11 play an important role in adhesive interactions occurring between growing axons. Cadherin-11 promote the fasciculation course of motor axon bundles [49] and the construction of neural networks [52] by regulating interaction of growth cones for neighboring axons. The up-regulated expression of Cdh11 gene and the increased translation of cadherin-11 protein in the treatment group are consistent with the observations of rapid and targeted growth of axons, which suggests that mechanical forces mediated by FMSPs can promote Cdh11 gene expression.

Csf1r gene encodes the receptor for colony stimulating factor 1. The colony stimulating factor 1 (Csf1) is a cytokine which controls the production, differentiation, and function of macrophages. This receptor mediates most of the biological effects of this cytokine. After a peripheral nerve lesion, the neuron undergoes a number of degenerative processes, the so-called Wallerian degeneration, followed by attempts at regeneration. Breakdown of the axon distal to the site of injury is initiated 48 to 96 h after transection. Deterioration of myelin begins, and the axon becomes disorganized. Macrophages, as immune cells, gathered around the damaged areas can phagocytose myelin and axonal debris [53] which is conducive to decrease inflammatory immune response[54–56], as well as promoted axonal regeneration by releasing a large number of regeneration related factors, including extracellular matrix

proteins, growth factors, cytokines and chemokines[31, 57–59]. Our results indicate that the combination of FMSPs and magnetic field can improve the biological function of Csf1 cytokines by up-regulating the expression of Csf1r gene, and in turn contribute to axonal regeneration through Csf1 dependent macrophages activation [60].

Ppp1r1c gene encodes protein phosphatase 1 (PP1) regulatory inhibitor subunit 1C, belongs to a group of PP1 inhibitory subunits that are themselves regulated by phosphorylation. PP1 is a major serine/threonine phosphatase that regulates a variety of cellular functions and play a critical role in the regulation of neuronal morphology. PP1 is proved to promote axonal growth by dephosphorylation of the microtubule-associated proteins [61]. However, Ppp1r1c as an up-regulated gene, contribute to the development of axon growth in the current study. The possible reason of this seemingly contradictory effect may be heterogeneity of samples between different experiments. There are few Ppp1r1c studies associated with axon growth. Thus, the potential molecular mechanism of Ppp1r1c for axon growth needs more evidences.

Conclusion

In summary, we have successfully designed and prepared a novel FMSPs for neural regeneration therapeutics. By virtue of their excellent biocompatibility and ability to interact with neural cells, the homemade FMSPs can be endocytosed into cells, transported along the axons, and then aggregated in the growth cones. Because of their high saturation magnetization, mechanical forces generated by FMSPs can promote the growth and elongation of axons under external magnetic fields, resulting in the realization of precisely and non-invasively remote manipulation of neurons regeneration. Furthermore, the mechanism of magnetic mechanical force on promoting axonal regeneration is studied by mRNA transcriptome sequencing and bioinformatics analysis. The results indicate that the combination of FMSPs and magnetic field can improve the biological function of Cadherin-11 and Csf1 by up-regulating the expression of Cdh11 and Csf1r genes, then in turn contribute to axonal regeneration. Since the manipulation of neuronal growth is of great significance in the fields of neural regeneration therapeutics, it is believed that our findings not only provide a powerful stimulator for axonal development, but also explore the signaling pathway between the mechanical force stimulation and the biological events of axon elongation.

Additional Files

Additional file 1 (. doc): Supplementary Information.

Additional file 2: Movie S1 (.avi). PC12 cells maintain active mitotic proliferation and neurites outgrowth after endocytosis of FMSPs. The arrows highlight the proliferating and differentiated cells.

Additional file 3: Movie S2 (.avi). FMSPs-treated DRG neurons show neurite outgrowth and formation of complex neuronal networks.

Additional file 4: Movie S3 (.mp4). FMSPs are transported along the axons and then aggregate in the growth cones.

Additional file 5: Movie S4 (.mp4). The neurites of PC12 cells treated with FMSPs tended to be arranged parallel to one another and grow preferentially along the direction of the magnetic field. The arrows highlight the neurites that directional growth.

Additional file 6: Movie S5 (.mp4). Dynamic growth process of DRG neurons axons in treatment group (FMSPs$^+$, M$^+$).

Additional file 7: Movie S6 (.mp4). Dynamic growth process of DRG neurons axons in FMSPs control group (FMSPs$^+$, M$^-$).

Additional file 8: Movie S7 (.mp4). Dynamic growth process of DRG neurons axons in magnetic field control group (FMSPs$^-$, M$^+$).

Additional file 9: Movie S8 (.mp4). Dynamic growth process of DRG neurons axons in blank control group (FMSPs$^-$, M$^-$).

Declarations

Ethics approval and consent to participate

Not applicable

Consent for publication

Not applicable

Availability of data and materials

All sequence data generated and analysed during the current study are available in the NCBI database under the project accession number PRJNA597946, (https://www.ncbi.nlm.nih.gov/sra/PRJNA597946).

Competing interests

The authors declare that they have no competing interests.

Funding

Authors' contributions

YW designed and carried out experiments and wrote the manuscript. BXL and SLD synthesized the $Fe_3O_4 \cdot$ Rhodamine 6G@PDA Superparticles with supervision from HZ. HX and TL obtained and analyzed data. JYR and JYZ participated in most experiments. LJL and YL proposed and supervised the project. All authors read and approved the final manuscript.

Author details

[1]Department of Hand Surgery, the First Hospital of Jilin University, Changchun 130021, P. R. China. [2]State Key Laboratory of Supramolecular Structure and Materials, College of Chemistry, Jilin University, Changchun 130012, P. R. China. [3]Institute of Translational Medicine, the First Hospital of Jilin University, Changchun 130021, P. R. China. [4]Departments of Geriatrics, the First Hospital of Jilin University, Changchun 130021, P. R. China.

Yang Wang, Email: wangy19851022@sina.com

Binxi Li, E-mail: bxli17@mails.jlu.edu.cn

Hao Xu, Email: xuhao_jlu@126.com

Shulin Du, Email: dusl1214@mails.jlu.edu.cn

Ting Liu, Email: liuting19850418@163.com

Jingyan Ren, Email: 413187467@qq.com

Jiayi Zhang, Email: 13944872076@163.com

Hao Zhang, Email: hao_zhang@jlu.edu.cn

Yi Liu, Email: yiliuchem@jlu.edu.cn

Laijin Lu, Tel: +86 431 84808260, Fax: +86 431 84808391, Email: lulaijin@hotmail.com

References

1. Isaacs J. Treatment of Acute Peripheral Nerve Injuries: Current Concepts. J Hand Surg Am. 2010;35:491-7.

2. Shoichet MS, Tate CC, Baumann MD, LaPlaca MC. Indwelling Neural Implants: Strategies for Contending with the In Vivo Environment. In: Reichert WM, editor. CRC Press. Boca Raton, FL; 2007. P. 221-44.

3. Franze K, Guck J. The Biophysics of Neuronal Growth. Rep Prog Phys. 2010;73:19.

4. Bray D. Axonal Growth in Response to Experimentally Applied Mechanical Tension. Dev Biol. 1984;102:379-89.

5. Kilinc D, Blasiak A, O'Mahony JJ, Lee GU. Low Piconewton Towing of CNS Axons Against Diffusing and Surface-Bound Repellents Requires the Inhibition of Motor Protein-Associated Pathways. Sci Rep. 2014; 4:7128.

6. Riggio C, Calatayud MP, Giannaccini M, Sanz B, Torres TE, Fernández-Pacheco R, Ripoli A, Ibarra MR, Dente L, Cuschieri A, Goya GF, Raffa V. The Orientation of the Neuronal Growth Process can be Directed via Magnetic Nanoparticles under an Applied Magnetic Field. Nanomedicine. 2014;10:1549-58.

7. Steketee MB, Moysidis SN, Jin XL, Weinstein JE, Pita-Thomas W, Raju HB, Iqbal S, Goldberg JL. Nanoparticle-mediated signaling endosome localization regulates growth cone motility and neurite growth. Proc Natl Acad Sci U S A. 2011;108:19042-7.

8. Marcus M, Karni M, Baranes K, Levy I, Alon N, Margel S, Shefi O. Iron oxide nanoparticles for neuronal cell applications: uptake study and magnetic manipulations. J Nanobiotechnology. 2016;14:37-48.

9. Riggio C, Calatayud MP, Hoskins C, Pinkernelle J, Sanz B, Torres TE, Ibarra MR, Wang L, Keilhoff G, Goya GF, Raffa V, Cuschieri A. Poly-l-lysine-coated magnetic nanoparticles as intracellular actuators for neural guidance. Int J Nanomedicine. 2012;7:3155-66.

10. Tay A, Kunze A, Murray C, Di Carlo D. Induction of Calcium Influx in Cortical Neural Networks by Nanomagnetic Forces. ACS Nano. 2016;10:2331-41.

11. Tay A, Di Carlo D. Magnetic Nanoparticle-Based Mechanical Stimulation for Restoration of Mechano-Sensitive Ion Channel Equilibrium in Neural Networks. Nano Lett. 2017;17:886-92.

12. Ge R, Li X, Lin M, Wang D, Li S, Liu S, Tang Q, Liu Y, Jiang J, Liu L, Sun H, Zhang H, Yang B. Fe_3O_4@polydopamine Composite Theranostic Superparticles Employing Preassembled Fe_3O_4 Nanoparticles as the Core. ACS Appl Mater Interfaces. 2016;8:22942-52.

13. Sun S, Zeng H. Size-Controlled Synthesis of Magnetite Nanoparticles. J Am Chem Soc. 2002;124:8204-5.

14. Zhuang J, Wu H, Yang Y, Cao YC. Controlling Colloidal Superparticle Growth through Solvophobic Interactions. Angew Chem Int Ed Engl. 2008;47:2208-12.

15. Bai F, Wang D, Huo Z, Chen W, Liu L, Liang X, Chen C, Wang X, Peng Q, Li Y. A Versatile Bottom-up Assembly Approach to Colloidal Spheres from Nanocrystals. Angew Chem Int Ed Engl. 2007;46:6650-3.

16. Tang L, Yang X, Yin Q, Cai K, Wang H, Chaudhury I, Yao C, Zhou Q, Kwon M, Hartman JA, Dobrucki IT, Dobrucki LW, Borst LB, Lezmi S, Helferich WG, Ferguson AL, Fan TM, Cheng J. Investigating the Optimal Size of Anticancer Nanomedicine. Proc Natl Acad Sci U S A. 2014;111:15344–9.

17. Tian HC, Liu JQ, Wei DX, Kang XY, Zhang C, Du JC, Yang B, Chen X, Zhu HY, Nuli YN, Yang CS. Graphene Oxide Doped Conducting Polymer Nanocomposite Film for Electrode-Tissue Interface. Biomaterials. 2014;35:2120-9.

18. Masand SN, Perron IJ, Schachner M, Shreiber DI. Neural Cell Type-Specific Responses to Glycomimetic Functionalized Collagen. Biomaterials. 2012;33:790-7.

19. Pinkernelle J, Calatayud P, Goya GF, Fansa H, Keilhoff G. Magnetic Nanoparticles in Primary Neural Cell Cultures are Mainly Taken Up by Microglia. BMC Neurosci. 2012;22:13-32.

20. Zhang K, Osakada Y, Vrljic M, Chen L, Mudrakola HV, Cui B. Single-Molecule Imaging of NGF Axonal Transport in Microfluidic Devices. Lab Chip. 2010;10: 2566-73.

21. Zhou N, Zhu SJ, Maharjan S, Hao ZY, Song YB, Zhao XH, Jiang YF, Yang B, Lu LJ. Elucidating the Endocytosis, Intracellular Trafficking, and Exocytosis of Carbon Dots in Neural Cells. RSC Adv. 2014;4:62086-95.

22. Kilinc D, Dennis CL, Lee GU. Bio-Nano-Magnetic Materials for Localized Mechanochemical Stimulation of Cell Growth and Death. Adv Mater. 2016;28:5672-80.

23. Taylor AM, Rhee SW, Tu CH, Cribbs DH, Cotman CW, Jeon NL. Microfluidic Multicompartment Device for Neuroscience Research. Langmuir. 2003;19:1551-6.

24. Park JW, Vahidi B, Taylor AM, Rhee SW, Jeon NL. Microfluidic Culture Platform for Neuroscience Research. Nat Protoc. 2006;1:2128-36.

25. Taylor AM, Blurton-Jones M, Rhee SW, Cribbs DH, Cotman CW, Jeon NL. A Microfluidic Culture Platform for CNS Axonal Injury, Regeneration and Transport. Nat Methods. 2005;2:599-605.

26. Taylor AM, Rhee SW, Jeon NL. Microfluidic Chambers for Cell Migration and Neuroscience Research. Methods Mol Biol. 2006;321:167-77.

27. Pertea M, Kim D, Pertea GM, Leek JT, Salzberg SL. Transcript-Level Expression Analysis of RNA-seq Experiments with HISAT, StringTie and Ballgown. Nat Protoc. 2016;11:1650-67.

28. Liao Y, Smyth GK, Shi W. FeatureCounts: an Efficient General Purpose Program for Assigning Sequence Reads to Genomic Features. Bioinformatics. 2014;30:923-30.

29. Love MI, Huber W, Anders S. Moderated Estimation of Fold Change and Dispersion for RNA-seq Data with DESeq2. Genome Biol. 2014;15:550.

30. Yu G, Wang LG, Han Y, He QY. ClusterProfiler: an R Package for Comparing Biological Themes Among Gene Clusters. OMICS. 2012;16:284-7.

31. Ashburner M, Ball CA, Blake JA, Botstein D, Butler H, Cherry JM, Davis AP, Dolinski K, Dwight SS, Eppig JT, Harris MA, Hill DP, Issel-Tarver L, Kasarskis A, Lewis S, Matese JC, Richardson JE, Ringwald M, Rubin GM, Sherlock G. Gene ontology: Tool for the Unification of Biology. The Gene Ontology Consortium. Nat Genet. 2000;25:25-9.

32. Foged C, Brodin B, Frokjaer S, Sundblad A. Particle Size and Surface Charge Affect Particle Uptake by Human Dendritic Cells in an in Vitro Model. Int J Pharm. 2005;298:315-22.

33. Thorek DL, Tsourkas A. Size, Charge and Concentration Dependent Uptake of Iron Oxide Particles by Non-Phagocytic Cells. Biomaterials. 2008;29:3583-90.

34. Connell JJ, Patrick PS, Yu Y, Lythgoe MF, Kalber TL. Advanced Cell Therapies: Targeting, Tracking and Actuation of Cells with Magnetic Particles. Regen Med. 2015;10:757-72.

35. Mahmoudi M, Hofmann H, Rothen-Rutishauser B, Petri-Fink A. Assessing the in Vitro and in Vivo Toxicity of Superparamagnetic Iron Oxide Nanoparticles. Chem Rev. 2012;112:2323-38.

36. Kim JA, Lee N, Kim BH, Rhee WJ, Yoon S, Hyeon T, Park TH. Enhancement of Neurite Outgrowth in PC12 Cells by Iron Oxide Nanoparticles. Biomaterials. 2011;32:2871-7.

37. Cao L, Wang X, Meziani MJ, Lu F, Wang H, Luo PG, Lin Y, Harruff BA, Veca LM, Murray D, Xie SY, Sun YP. Carbon dots for multiphoton bioimaging. J Am Chem Soc. 2007;129:11318-9.

38. Goh EJ, Kim KS, Kim YR, Jung HS, Beack S, Kong WH, Scarcelli G, Yun SH, Hahn SK. Bioimaging of hyaluronic acid derivatives using nanosized carbon dots. Biomacromolecules. 2012;13:2554-61.

39. Liu C, Zhang P, Zhai X, Tian F, Li W, Yang J, Liu Y, Wang H, Wang W, Liu W. Nano-carrier for gene delivery and bioimaging based on carbon dots with PEI-passivation enhanced fluorescence. Biomaterials. 2012;33:3604-13.

40. Baker SN, Baker GA. Luminescent carbon nanodots: emergent nanolights. Angew Chem Int Ed Engl. 2010;49:6726-44.

41. Mailänder V, Landfester K. Interaction of nanoparticles with cells. Biomacromolecules. 2009;10:2379–400.

42. Pisanic TR, Blackwell JD, Shubayev VI, Fiñones RR, Jin S. Nanotoxicity of iron oxide nanoparticle internalization in growing neurons. Biomaterials. 2007;28:2572-81.

43. Verma A, Stellacci F. Effect of surface properties on nanoparticle-cell interactions. Small. 2010;6:12-21.

44. Wang J, Byrne JD, Napier ME, DeSimone JM. More effective nanomedicines through particle design. Small. 2011;7:1919-31.

45. Hsu CY, Uludağ H. Cellular uptake pathways of lipid-modified cationic polymers in gene delivery to primary cells. Biomaterials. 2012;33:7834-48.

46. Jiang X, Röcker C, Hafner M, Brandholt S, Dörlich RM, Nienhaus GU. Endo-and exocytosis of zwitterionic quantum dot nanoparticles by live HeLa cells. ACS Nano. 2010;4:6787-97.

47. Kerstein PC, Nichol IV RH, Gomez TM. Mechanochemical Regulation of Growth Cone Motility. Front Cell Neurosci. 2015;9:244.

48. Fass JN, Odde DJ. Tensile force-dependent neurite elicitation via anti-beta 1 integrin antibody-coated magnetic beads. Biophys J. 2003;85:623-36.

49. Marthiens V, Gavard J, Padilla F, Monnet C, Castellani V, Lambert M, Mège RM. A Novel Function for Cadherin-11 in the Regulation of Motor Axon Elongation and Fasciculation. Mol Cell Neurosci.

2005;28:715-26.

50. Marthiens V, Gavard J, Lambert M, Mège RM. Cadherin-Based Cell Adhesion in Neuromuscular Development. Biol Cell. 2002;94:315-26.

51. Marthiens V, Padilla F, Lambert M, Mege RM. Complementary Expression and Regulation of Cadherins 6 and 11 During Specific Steps of Motoneuron Differentiation. Mol Cell Neurosci. 2002;20:458-75.

52. Hirano S, Suzuki ST, Redies C. The Cadherin Superfamily in Neural Development: Diversity, Function and Interaction with Other Molecules. Front Biosci. 2003;8:d306-355.

53. Filbin MT. Myelin-Associated Inhibitors of Axonal Regeneration in the Adult Mammalian CNS. Nat Rev Neurosci. 2003;4:703-13.

54. Farah MH, Pan BH, Hoffman PN, Ferraris D, Tsukamoto T, Nguyen T, Wong PC, Price DL, Slusher BS, Griffin JW. Reduced BACE1 Activity Enhances Clearance of Myelin Debris and Regeneration of Axons in the Injured Peripheral Nervous System. J Neurosci. 2011;31:5744-54.

55. Chiu H, Zou Y, Suzuki N, Hsieh YW, Chuang CF, Wu YC, Chang C. Engulfing Cells Promote Neuronal Regeneration and Remove Neuronal Debris Through Distinct Biochemical Functions of CED-1. Nat Commun. 2018;9:4842.

56. Vargas ME, Watanabe J, Singh SJ, Robinson WH, Barres BA. Endogenous Antibodies Promote Rapid Myelin Clearance and Effective Axon Regeneration After Nerve Injury. Proc Natl Acad Sci U S A. 2010;107:11993-8.

57. Chen P, Piao X, Bonaldo P. Role of Macrophages in Wallerian Degeneration and Axonal Regeneration after Peripheral Nerve Injury. Acta Neuropathol. 2015;130:605-18.

58. Gaudet AD, Popovich PG, Ramer MS. Wallerian Degeneration: Gaining Perspective on Inflammatory Events after Peripheral Nerve Injury. J Neuroinflammation. 2011;8:110.

59. Myers RR, Heckman HM, Rodriguez M. Reduced Hyperalgesia in Nerve-Injured WLD Mice: Relationship to Nerve Fiber Phagocytosis, Axonal Degeneration, and Regeneration in Normal Mice. Exp Neurol. 1996;141:94-101.

60. Forget MA, Voorhees JL, Cole SL, Dakhlallah D, Patterson IL, Gross AC, Moldovan L, Mo X, Evans R, Marsh CB. Macrophage Colony-Stimulating Factor Augments Tie2-Expressing Monocyte Differentiation, Angiogenic Function, and Recruitment in a Mouse Model of Breast Cancer. PLoS One. 2014;9:e98623.

61. Bielas SL, Serneo FF, Chechlacz M, Deerinck TJ, Perkins GA, Allen PB, Ellisman MH, Gleeson JG. Spinophilin Facilitates Dephosphorylation of Doublecortin by PP1 to Mediate Microtubule Bundling at the Axonal Wrist. Cell. 2007;129:579-91.

Figures
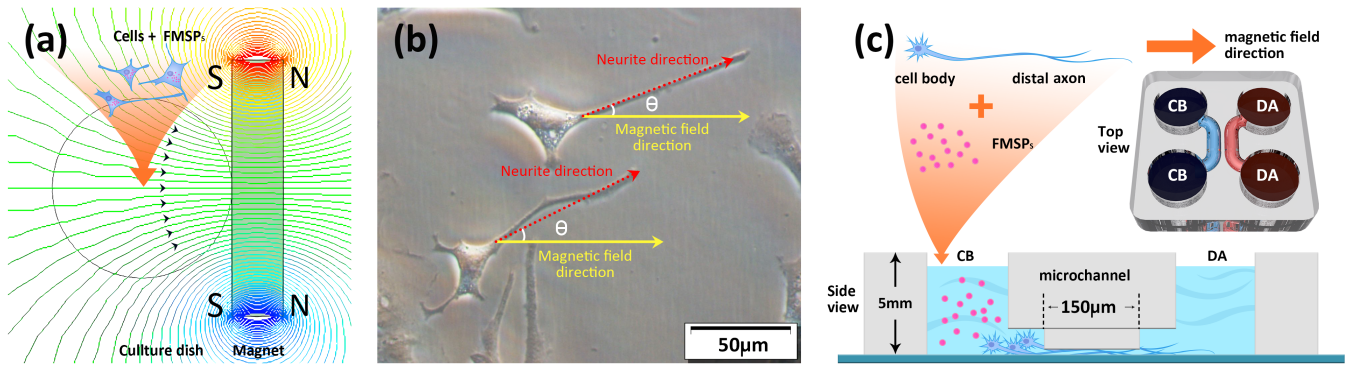
Figure 1

Magnetic applicator and experimental set-up of neurite outgrowth. (a) Schematic illustration of the gradient magnetic field generated by the perpetual cuboid neodymium magnet applied to the cells at the center of the dish. (b) The angles θ between the long axis of the neurites (red dotted line) and the direction of magnetic field (yellow solid line) (0<θ<π). (c) Schematic illustration of two-compartment microfluidic device for separating axons from cell bodies in DRG neurons culture.
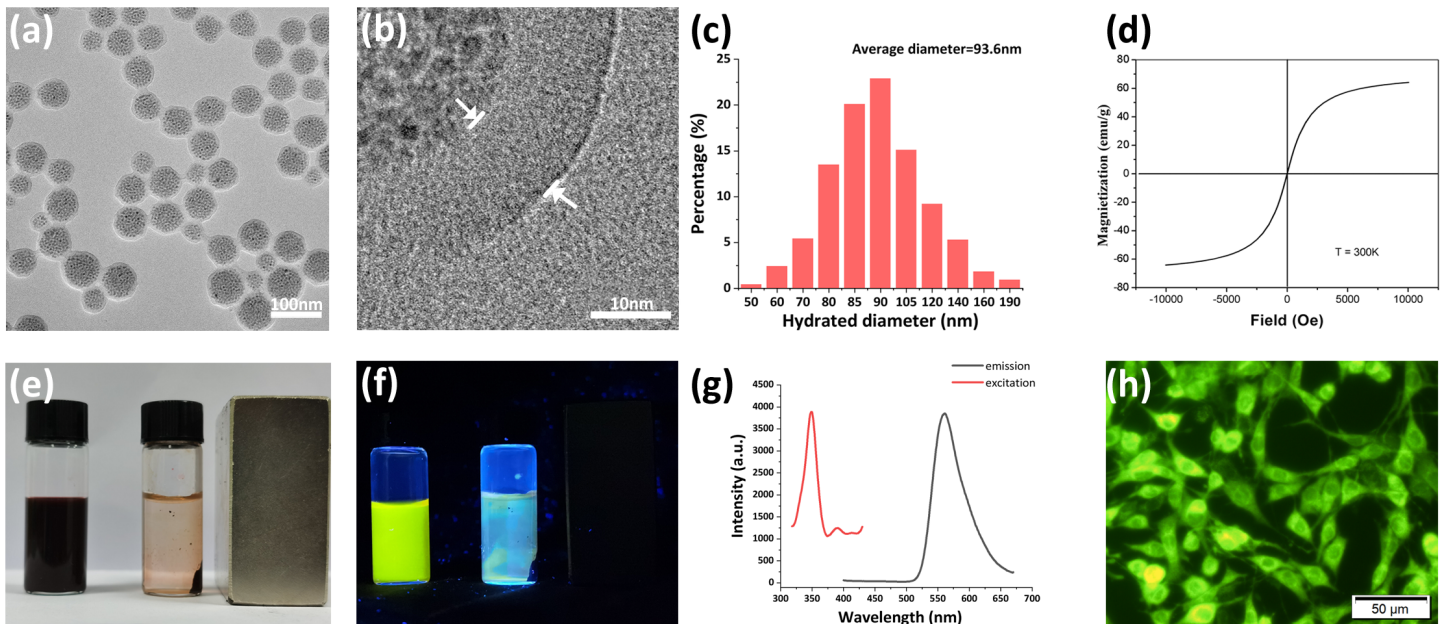

Figure 2

TEM (a) and HRTEM (b) images of FMSPs. (c) Size distribution of FMSPs. (d) Magnetic curves of FMSPs. Optical photograph (e) and fluorescent photograph (f) of FMSPs in the absence and presence of external magnetic field. (g) PL emission and excitation spectra of FMSPs. (h) Fluorescence microscopy image of PC12 cells after incubation with FMSPs.
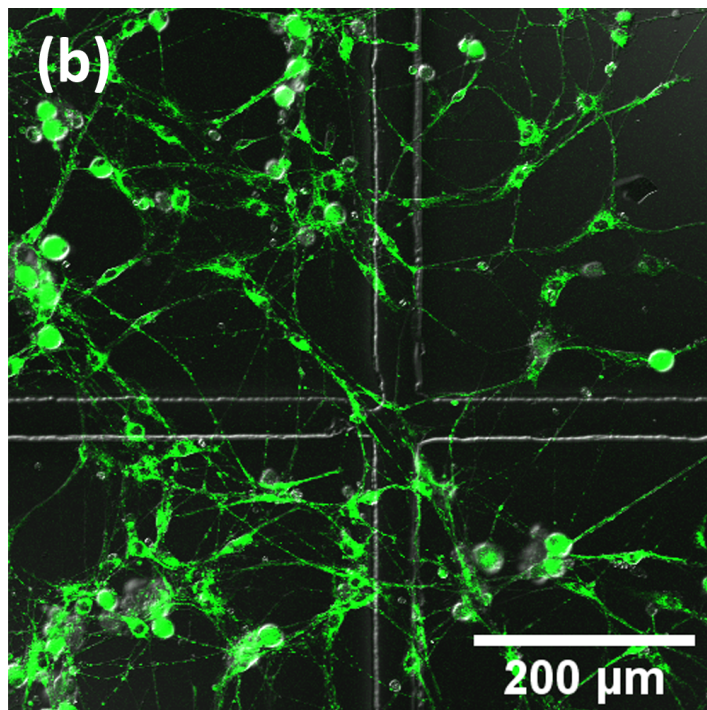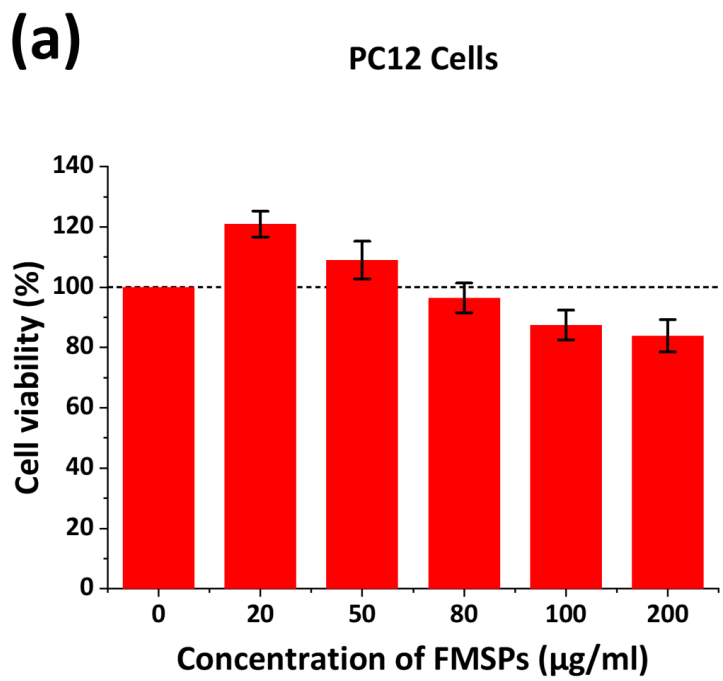
Figure 3

Cytotoxicity of FMSPs in PC12 cells. (a) Viability of PC12 cell after 24 h co-culture with different concentrations of FMSPs. (b) Outgrowth of FMSPs-treated DRG neurons after incubation with FMSPs (10 µg/ml) for 72h .
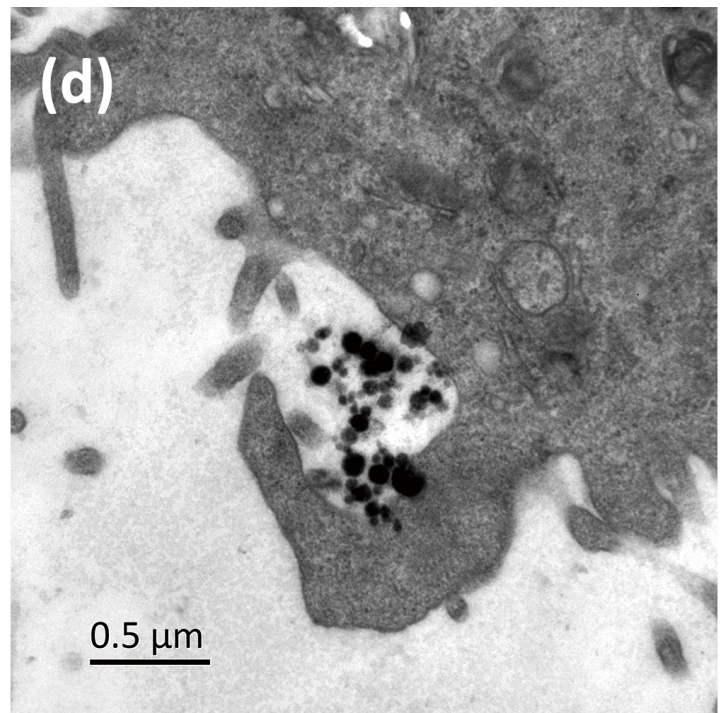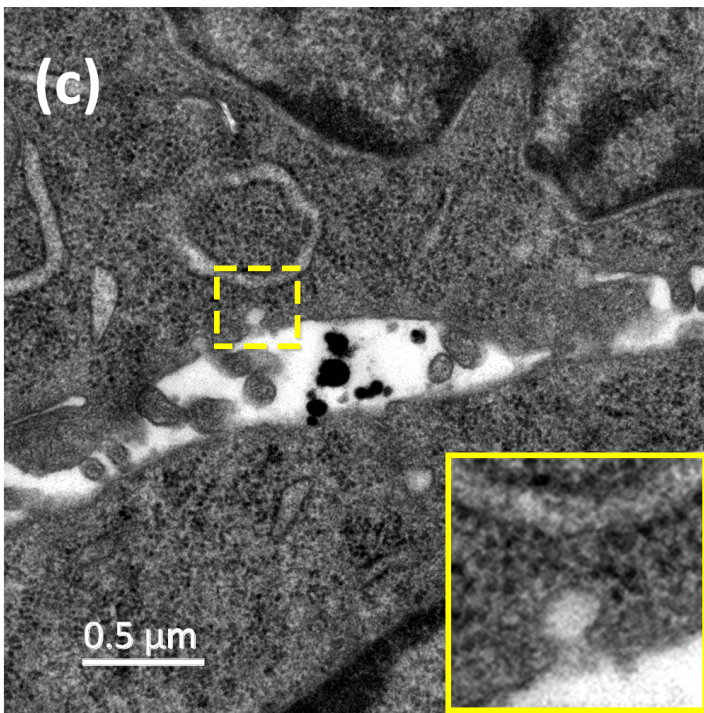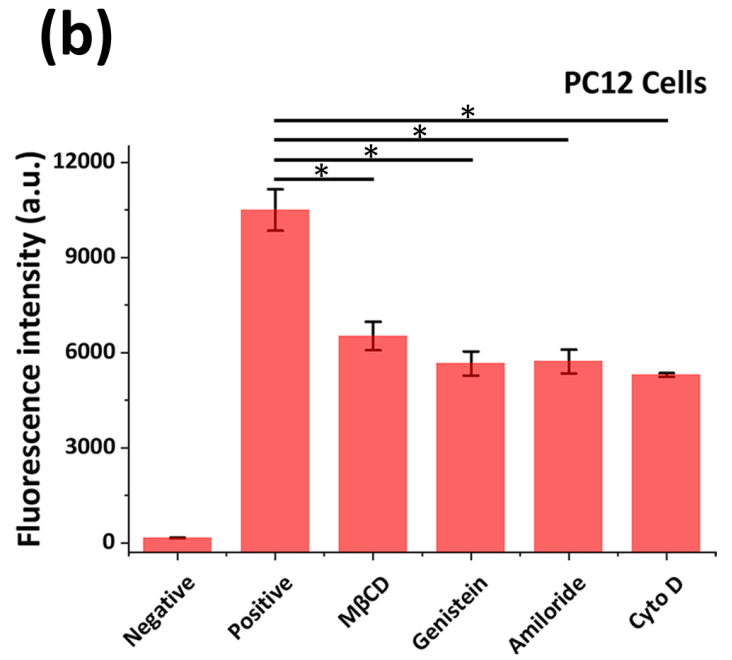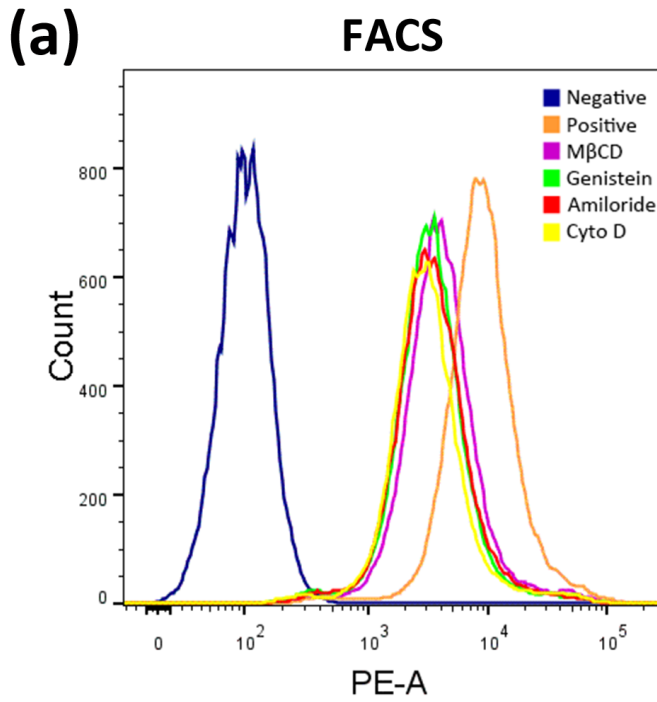
Figure 4

(a) FACS analysis for determining the endocytic pathways of FMSPs in PC12 cells. (b) Intracellular fluorescent intensity of PC12 cells in the presence of different endocytosis inhibitors. (c) TEM image of caveolae-mediated endocytosis. Insert is the magnified representative area (yellow box) of the flask-shaped structure of caveolae (60−80 nm). (d) TEM image of micropinocytosis. The diameter and depth of the invagination structures conforms to the characteristic features of micropinocytosis. *P<0.05.
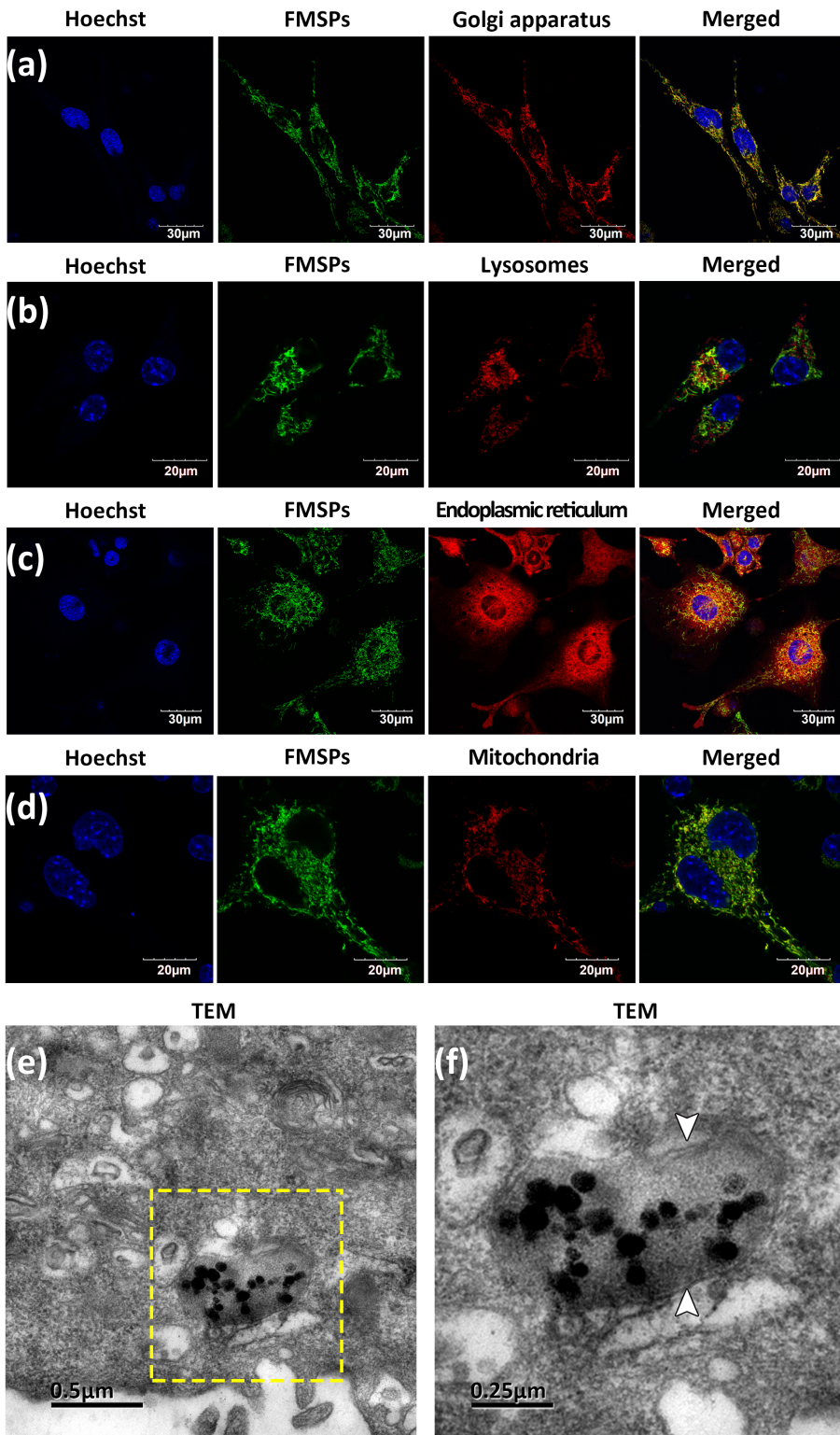
Figure 5

CLSM images of the colocalization of FMSPs with Golgi apparatus (a), lysosomes (b), endoplasmic reticulum (c) and mitochondria (d). (e) TEM image of FMSPs distributed in mitochondria. (f) The enlarged local area of (e) to demonstrate the FMSPs with high electron-dense and the characteristic double-layer membrane structure (white arrows) of mitochondria.
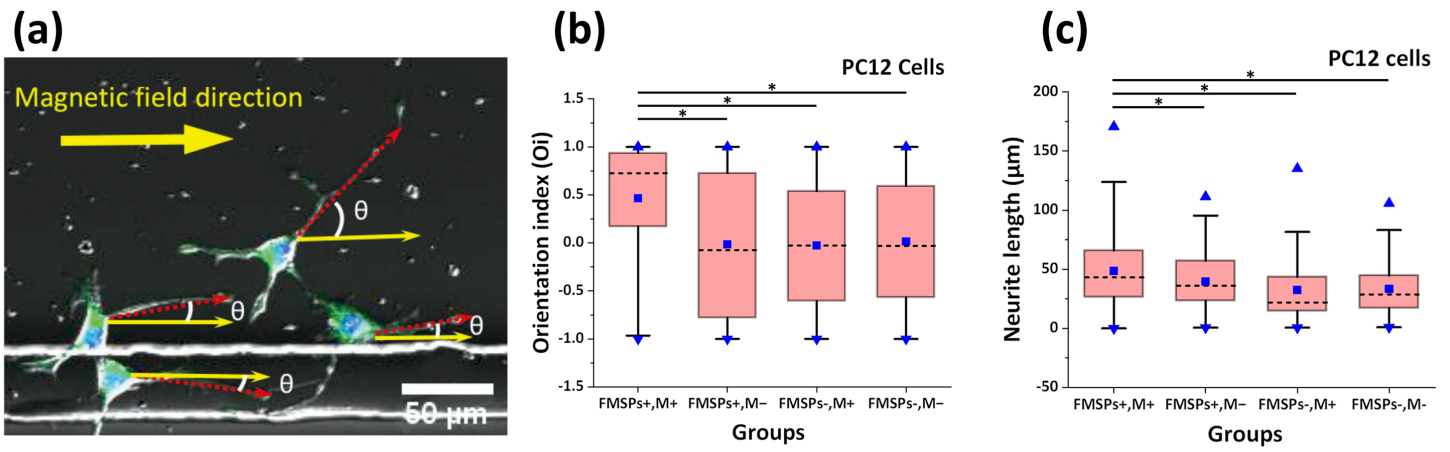
Figure 6

(a) Magnetic guidance outgrowth of PC12 cells neurites in directional orientation in the treatment group (FMSPs+, M+). The value of the orientation index (b) and neurites length (c) in the treatment group compared to the control groups. The box-plot shows the median (whiskers), interquartile ranges (boxes), and 5−95% percentiles (line). The square represents the mean value and triangles represent maximum and minimum. *P<0.05.
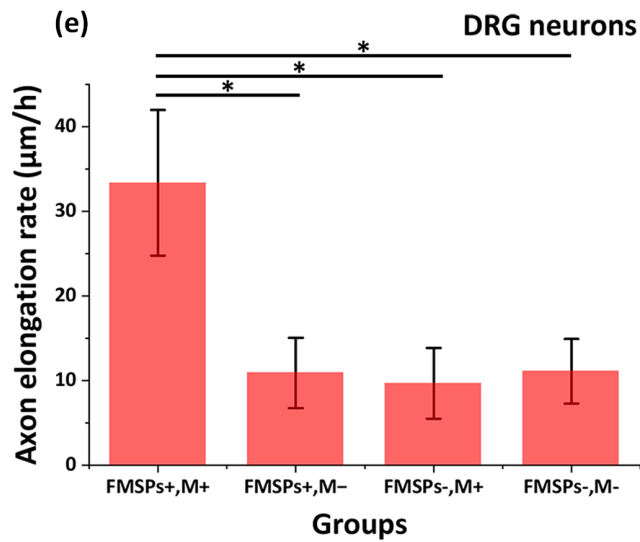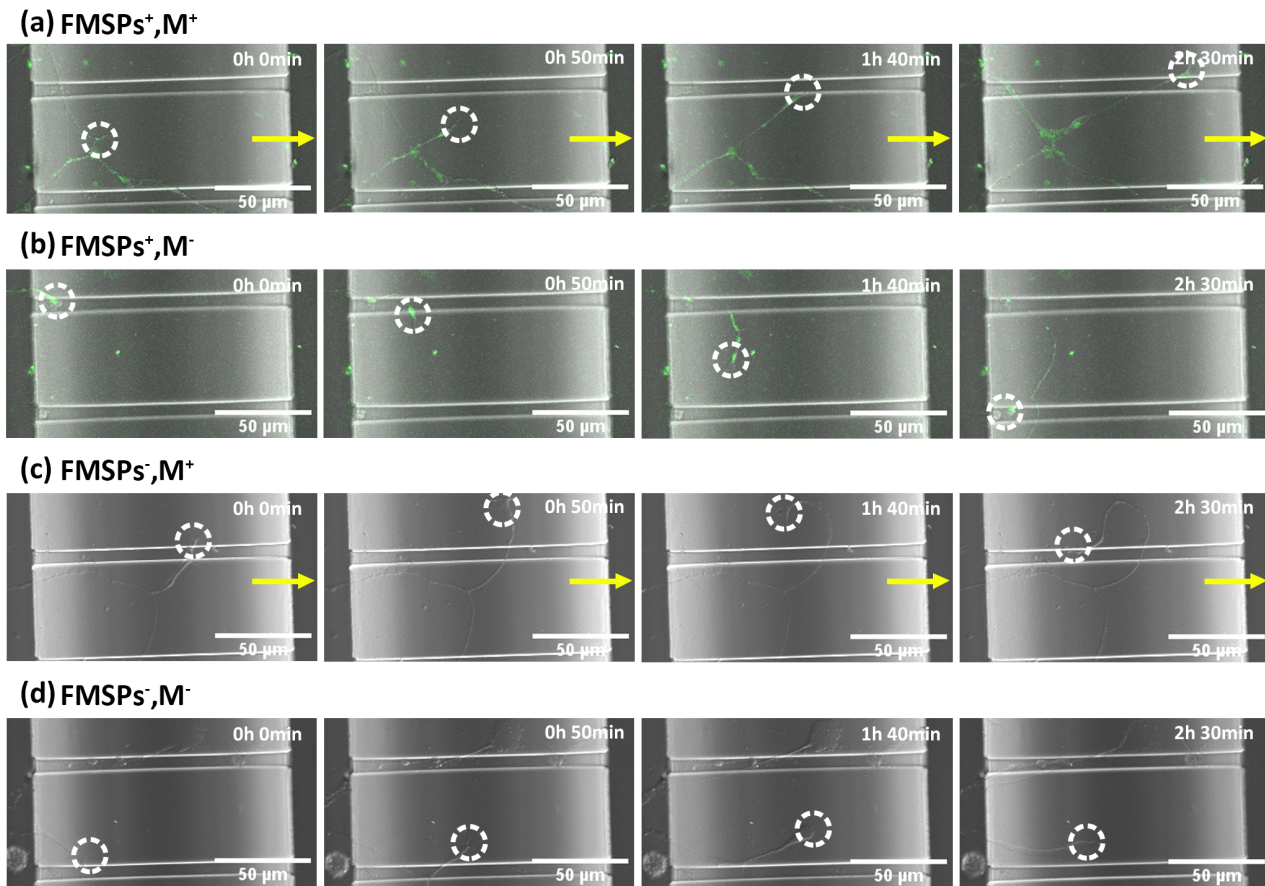
Figure 7

Time-lapse imaging of growth cone motility and axon elongation of DRG neurons in (a) treatment group (FMSPs+, M+), (b) FMSPs control group (FMSPs+, M-), (c) magnetic field control group (FMSPs -, M+) and (d) blank control group (FMSPs-, M-). (e) The average elongation rate of the axons in the treatment group compared to the control groups. The yellow arrows represent the direction of magnetic field. The

white circles highlight the growth cones. The images were captured at an interval of 50min in panel a-d. *P<0.05.


(a)

(b)

(c)

Gene Ontology
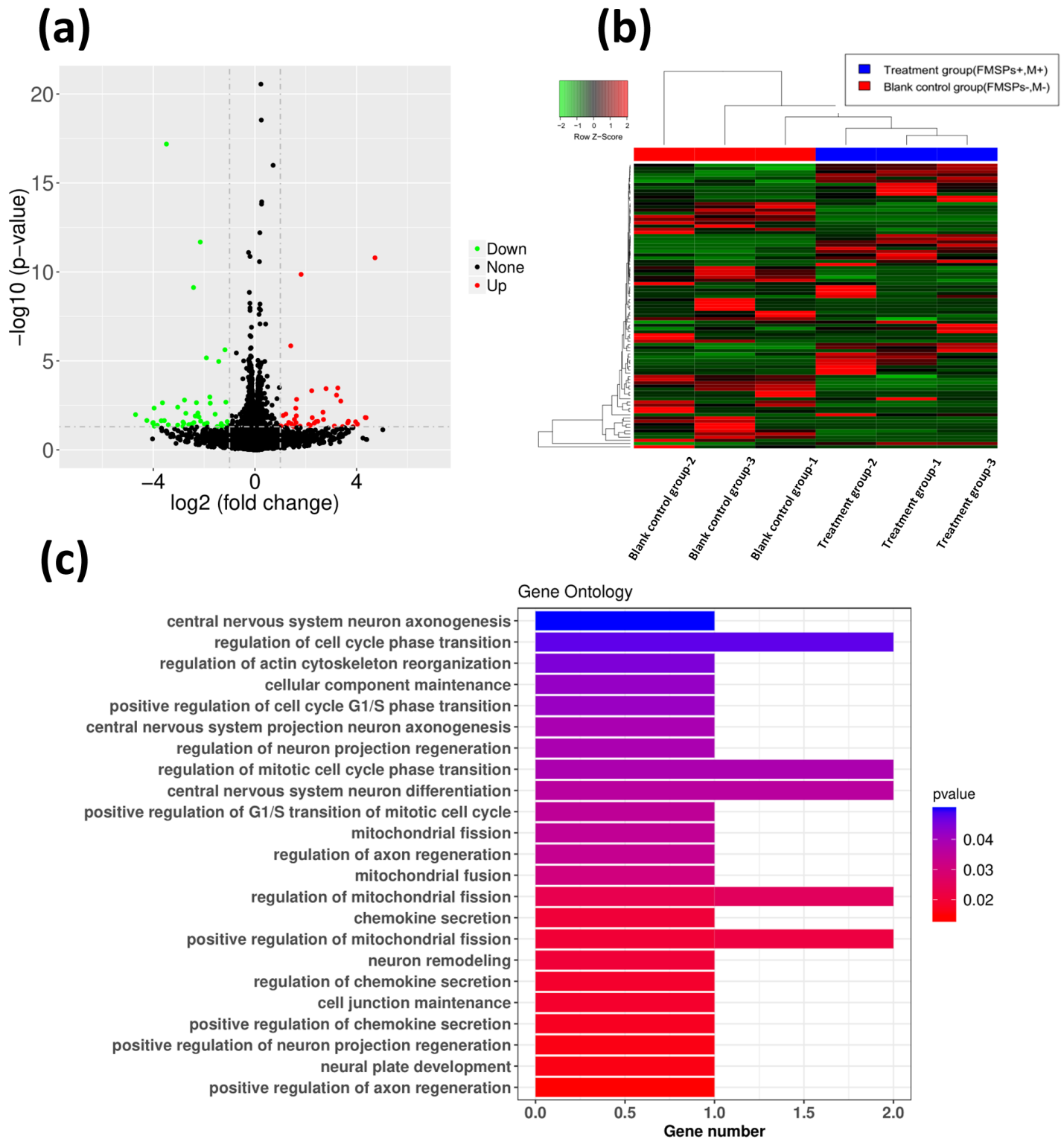
Figure 8

Screening differentially expressed mRNA. (a) The volcano plot of all differentially expressed mRNA. Red and green dots represent up- and down-regulated mRNA, respectively. (b) Heat map visualization of the

patterns of expression change for the significantly differentially expressed mRNA between treatment and blank control groups. (c) Gene ontology enrichment analysis associated with axon growth.
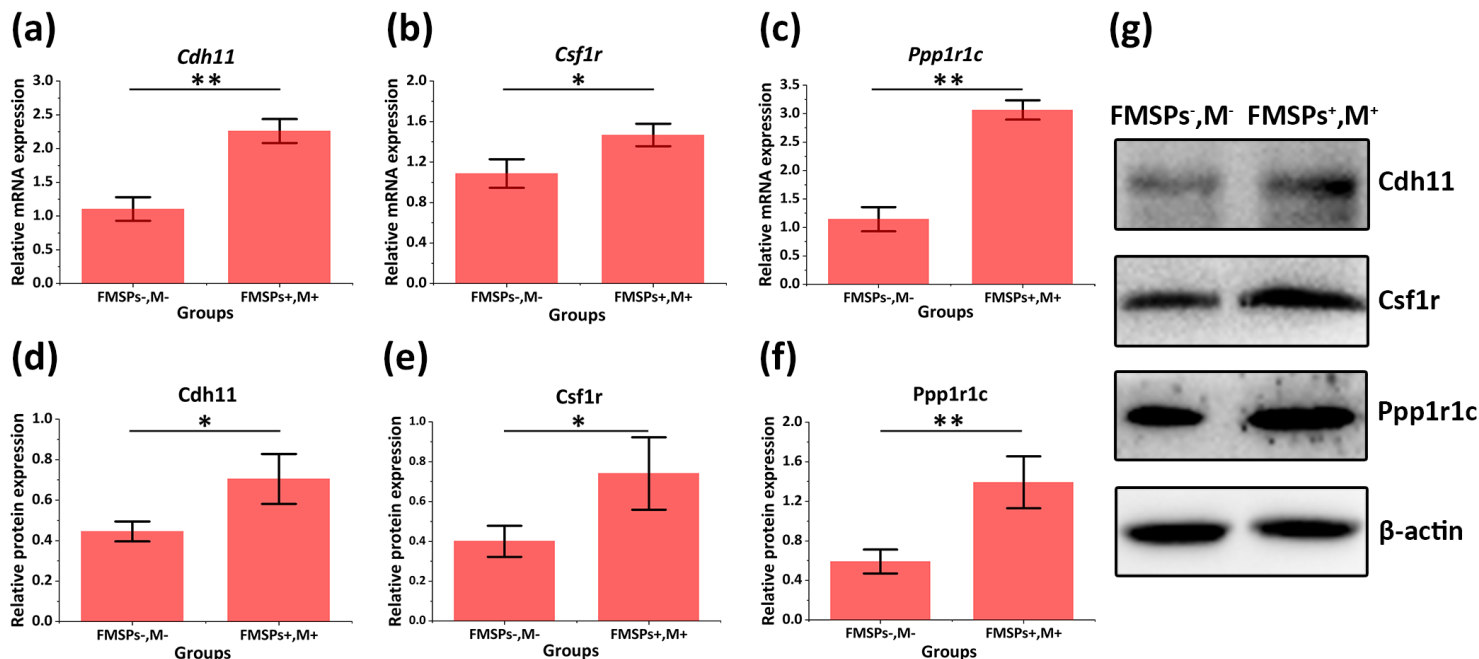

Figure 9

RT-qPCR and western blot verification of differentially expressed mRNAs. (a-c) The RT-qPCR validation of the expression level of Cdh11, Csf1r and Ppp1r1c were significantly up-regulated in treatment group compared with blank control group. (d-g) Western blot validation of the protein level of Cdh11, Csf1r, and Ppp1r1c were remarkably increased in treatment group compared with blank control group. *P<0.05, **P<0.01.

Supplementary Files

This is a list of supplementary files associated with this preprint. Click to download.

- Additionalfile5.MovieS4..mp4
- Additionalfile2.MovieS1..avi
- Additionalfile7.MovieS6..mp4
- Additionalfile1.SupplementaryInformation..docx
- Additionalfile6.MovieS5..mp4
- Additionalfile4.MovieS3..mp4
- Additionalfile8.MovieS7..mp4
- Additionalfile3.MovieS2..avi
- Additionalfile9.MovieS8..mp4